Electronic Supplementary Material (ESI) for Dalton Transactions.
This journal is © The Royal Society of Chemistry 2022

Heterometallic Chiral [$Mn_{13}Cu_8$] Single-Molecule Magnets

Zhiwei Peng,[a] Shu Li,[a] Ao Li,[a] Jiaming Liao,[a] Yiman Wang,[a] Xudong Li,[a] Wei Meng*[a] and Jian Zhang*[b]

[a] Hunan Provincial Key Lab of Dark Tea and Jin-Hua, Departmet of Material & Chemical Engineering, Hunan City University, Yiyang, 413000, P. R. China.

[b] State Key Laboratory of Structural Chemistry, Fujian Institute of Research on the Structure of Matter, Chinese Academy of Sciences, Fuzhou, Fujian 350002, P. R. China.
E-mail: mengw198503@163.com and zhj@fjirsm.ac.cn

CONTENTS

Section 1 Experimental Section
Table S1. Bond-Valence Sums for the Mn and Cu Atoms of Complexes L-**1**
Table S2. Crystal data and structure refinement for complexes L-**1** and D-**1**
Table S3. Selected bond distances (Å) and bond angles (°) in L-**1**

Section 2 Supplementary Structural Figures.
Figure S1. Schematic view of the coordination modes a, b and c of the tartrate ligands in D-**1**. (Cu^{II} blue, Mn^{III} yellow, Mn^{II} green, O red, C gray, hydrogen atoms omitted for clarity)
Figure S2. Each $\{Mn_{13}Cu_8\}$ cluster is connected to eight nearest neighbor clusters, creating a 3D network of D-**1**. The green disordered tetradecahedron represents the $\{Mn_{13}\}$ core. a) the packing arrangement viewed along *a*-axis, b) the packing arrangement viewed along *b*-axis, c) the packing arrangement viewed along *c*-axis. (Cu^{II} blue, Mn^{III} yellow, Mn^{II} green, O red, C gray, hydrogen atoms omitted for clarity)
Figure S3. Ball-and-stick representation the 3D supramolecular assembly of D-**1** viewed along *a*-axis. (Cu^{II} blue, Mn^{III} yellow, Mn^{II} green, O red, C gray, Na black, K pink, hydrogen atoms omitted for clarity)
Figure S4. The $\{Mn_{12}\}$ irregular tetradecahedron with a central MnII in D-**1**. (Mn^{III} yellow, Mn^{II} green)
Figure S5. Space-filling representation of D-**1**. (Cu^{II} blue, Mn^{III} yellow, Mn^{II} green, O red, C gray, hydrogen atoms omitted for clarity)
Section 3 Supplementary Physical Characterization
Figure S6. IR spectrum of L-**1**.
Figure S7. IR spectrum of D-**1**.
Figure S8. CD spectra of L-**1** and D-**1** in a 0.5 M NaOAc/HOAc buffer solution at pH 5.5.
Figure S9. CD spectra of L-(+)- and of D-(-)-tartaric acid in water.
Figure S10. Variable temperature dc susceptibility data for D-**1** in a field of 2000 Oe from 2 – 300 K in log scale.
Figure S11. Variable temperature dc susceptibility data for L-**1** in a field of 2000 Oe from 2 – 300 K (top). Magnetisation versus field plots at temperatures of 1.8, 2.5, 5.0 and 10 K for L-**1** (bottom).
Figure S12. Temperature dependent in-phase susceptibility signals D-**1** in a 0 Oe dc applied magnetic field, in the temperature range 1.8 – 3.0 K.
Figure S13. The temperature-dependence of in phase (top) and out-of-phase (middle) magnetization susceptibility of L-**1** at different frequencies by SQUID VSM. The reversed energy barrier fitting plot with $\ln(\chi'' / \chi') = \ln(\omega\tau_0) + U/k_BT$ (bottom). The energy barrier is ca. U =19 (±4) K and $\tau_0 = 2.0\ (\pm 0.3) \times 10^{-9}$ s.
Figure S14. Frequency dependent in-phase (top) and out-of-phase (bottom) susceptibility signals for L-**1** in a 0 Oe dc applied magnetic field, in the temperature range 1.8 – 3.0 K.

Figure S15. Frequency dependent in-phase (top) and out-of-phase (bottom) susceptibility signals for D-**1** in a 0 Oe dc applied magnetic field, in the temperature range 1.8 – 3.0 K.
Figure S16. TGA of L-**1**.
Figure S17. TGA of D-**1**.
Figure S18. Simulated and observed powder X-ray diffraction (PXRD) of L-**1**.
Figure S19. Simulated and observed powder X-ray diffraction (PXRD) of D-**1**.
Figure S20. The EDS characterization for L-**1**.
Figure S21. The EDS characterization for D-**1**.

Section 1 Experimental Section

1. Materials and Methods:

All of the reagents employed were commercially available and were used without further purification. The infrared (IR) spectra were recorded (400−4000 cm^{-1} region) on a Nicolet Nexus 670 FTIR spectrometer using KBr pellets. Thermogravimetric analysis (TGA) measurements were carried out using a DSC/TG pan A1203 system in N_2 flow with a heating rate of 10 ℃ min^{-1}. Elemental analyses were performed (C, H, N) by Thermo Scientific FLASH 2000 elemental analyzer; Cu, Mn, K and Na were analyzed on a Varian (720) ICP atomic emission spectrometer. Powder X-ray diffraction (PXRD) patterns were collected at room temperature on a Rigaku D/Max 2500 diffractometer. Variable-temperature direct current (dc) was carried out at Nanjing University using a Quantum Design MPMS-XL-7 SQUID magnetometer equipped with a 7 T magnet and operating in the 1.8−300 K range. Alternating current (ac) magnetic susceptibility data was carried out at Nanjing University using the SQUID PPMS. Dc and ac magnetic measurements were collected by restraining the sample in eicosane in order to prevent torquing due to its magnetic anisotropy.

2. Synthesis of L-1 and D-1:

L-**1**: A mixture of $Cu(OAc)_2 \cdot H_2O$ (199 mg, 1 mmol), $Mn(OAc)_2 \cdot 4\ H_2O$ (245 mg, 1 mmol), and L-(+)-tartaric acid (150 mg, 1 mmol) was dissolved in a sodium acetate/acetic acid buffer solution (pH 5.5, 0.5 M NaOAc/HOAc, 10 mL). K_2CO_3 (4 ml, 1 M) and HCOONa (1 ml, 1 M) were gradually added while stirring. The mixture was stirred at room temperature for 12 h. Then the resulting black solution was filtered and the filtrate was left undisturbed at ambient temperature. After several days, the black needle crystals were obtained by filtration. The yield is 10% based on copper. Anal. calcd for $C_{49.7}H_{63.5}Cu_8Mn_{13}K_4Na_6O_{101.7}$ (L-**1**): C 15.69, H 1.67, Cu 13.36, Mn 18.77, K 4.11, Na 3.63. Found: C 15.94, H 1.65, Cu 13.26, Mn 18.65, K 4.67, Na 4.42. IR (KBr, cm^{-1}): 3426 s, 1630 s, 1365 s, 1222 w, 1121 m, 1085 m, 1040 m, 953 w, 902 w, 825 m, 744 m, 678 w, 633 w, 574 w, 511 w. D-**1** was prepared in a similar fashion to L-**1** except that D-(-)-tartaric acid was used instead of L-(+)-tartaric

acid (yield 10 % based on copper). Anal. calcd for $C_{49.7}H_{69.3}Cu_8Mn_{13}K_4Na_6O_{104.6}$ (D-**1**): C 15.48, H 1.97, Cu 13.18, Mn 18.52, K 4.05, Na 3.58. Found: C 15.98, H 1.67, Cu 13.23, Mn 18.59, K 4.64, Na 4.50. IR (KBr, cm^{-1}): 3431 s, 1637 s, 1366 s, 1220 w, 1126 m, 1084 m, 1042 m, 959 w, 907 w, 823 m, 740 m, 677 w, 635 w, 573 w, 510 w.

3. Crystallography:

The crystal data for L-**1** was collected at 293 K on a Smart Apex II CCD with graphite-monochromated $Mo_{K\alpha}$ radiation (λ = 0.71073Å). Suitable crystals were affixed to the end of a glass fiber using silicone grease and transferred to the goniostat. The crystal data for D-**1** was collected on a Bruker DUO diffractometer using Mo Kα radiation (λ = 0.71073 Å) and an APEXII CCD area detector. Suitable crystals were attached to glass fibers using silicone grease and transferred to the goniostat where they were cooled to 100 K for data collection. The structures of L-**1** were solved by the direct method and refined by the full-matrix least-squares method on F^2 using the *SHELXT 2014/5* and *SHELXL-2018/3* crystallographic software package. The D-**1** was solved and refined in *SHELXT 2014/5* and *SHELXL-2018/3*, using full-matrix least-squares refinement. The non-H atoms were refined with anisotropic thermal parameters and all of the H atoms were calculated in idealized positions and refined riding on their parent atoms. Crystallographic data and structural refinements for compounds L-**1** and D-**1** are summarized in Table S1. More details on the crystallographic studies as well as atomic displacement parameters are given in the CIF files. All carbon-bonded hydrogen atoms were placed in geometrically calculated positions, and hydrogen atoms in water molecules were not assigned or directly included in the molecular formula. In addition, CCDC-1951508 (L-**1**) and CCDC-1951511 (D-**1**) contain the supplementary crystallographic data for this paper. These data can be obtained free of charge from the Cambridge Crystallographic Data Centre via http://www.ccdc.cam.ac.uk/data_request/cif.

Table S1. Bond-Valence Sums for the Mn and Cu Atoms of Complexes L-**1** [a]

atom	Mn^{II}	Mn^{III}	atom	Cu^{I}	Cu^{II}
Mn1	1.62	1.49	Cu1	1.91	2.12
Mn2	3.08	2.82	Cu2	1.83	2.04
Mn3	3.25	2.97	Cu3	1.70	1.89
Mn4	3.19	2.91	Cu4	1.74	1.93
Mn5	3.19	2.91	Cu5	1.84	2.05
Mn6	3.18	2.91	Cu6	1.79	1.99
Mn7	3.19	2.92	Cu7	1.75	1.96
Mn8	3.17	2.90	Cu8	1.80	2.00
Mn9	3.09	2.83			
Mn10	3.08	2.82			
Mn11	3.28	3.00			
Mn12	3.26	2.98			
Mn13	3.16	2.89			

[a]The underlined value is closest to the charge it was calculated. The oxidation state is the nearest whole number to the underlined value.

Table S2. Crystal data and structure refinement for complexes L-**1** and D-**1**

complexes	L-**1**	D-**1**
empirical formula	$C_{49.7}H_{63.5}Cu_8Mn_{13}K_4Na_6O_{101.7}$	$C_{49.7}H_{69.3}Cu_8Mn_{13}K_4Na_6O_{104.6}$
fw	3804.82	3857.04
cryst syst	Triclinic	Triclinic
space group	P1	P1
a [Å]	13.0683(7)	13.0061(5)
b [Å]	15.7834(10)	15.9364(6)
c [Å]	16.6333(11)	16.6526(6)
α [deg]	114.266(3)	114.136(1)
β [deg]	99.410(3)	99.411(1)
γ [deg]	102.907(3)	102.301(1)
V [Å^3]	2920.1(3)	2953.44(2)
Z	1	1
Dcalcd [g/cm^{-3}]	2.152	2.155
μ [mm^{-1}]	3.065	3.034
F(000)	1853	1880
Flack parameter	0.002(8)	0.06(2)
goodness-of-fit on F^2	1.041	1.033
R indices (all data)	R_1 = 0.0619 wR_2 = 0.1688(20346)	R_1 = 0.0491 wR_2 = 0.1412(14780)
CCDC	1951508	2104879

Section 2: Supplementary Structural Figures

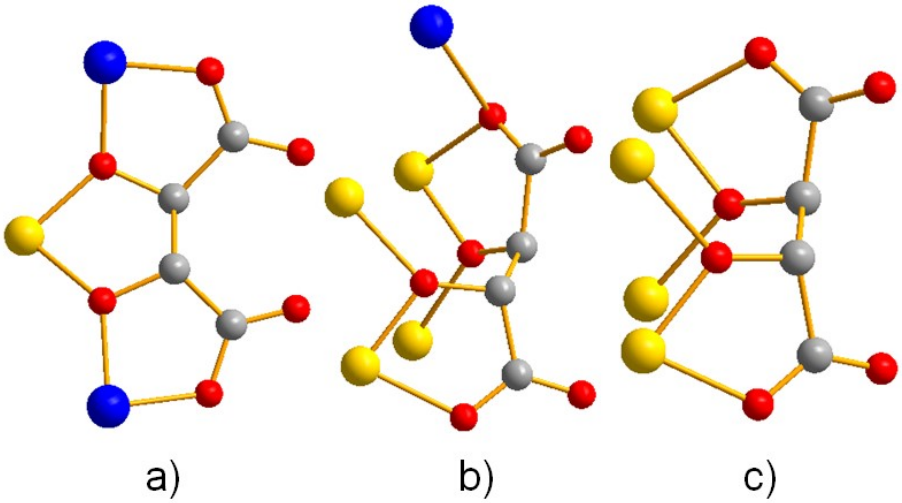

Figure S1. Schematic view of the coordination modes a, b and c of the tartrate ligands in D-**1**. (Cu^{II} blue, Mn^{III} yellow, Mn^{II} green, O red, C gray, hydrogen atoms omitted for clarity)

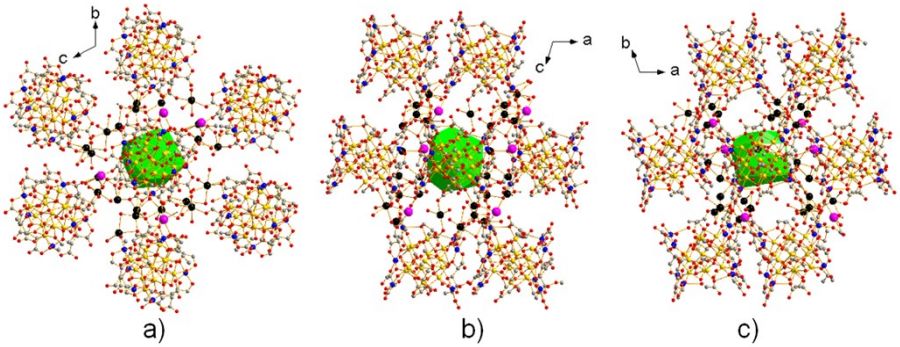

Figure S2. Each $\{Mn_{13}Cu_8\}$ cluster is connected to eight nearest neighbor clusters, creating a 3D network of D-**1**. The green disordered tetradecahedron represents the $\{Mn_{13}\}$ core. a) the packing arrangement viewed along *a*-axis, b) the packing arrangement viewed along *b*-axis, c) the packing arrangement viewed along *c*-axis. (Cu^{II} blue, Mn^{III} yellow, Mn^{II} green, O red, C gray, hydrogen atoms omitted for clarity)

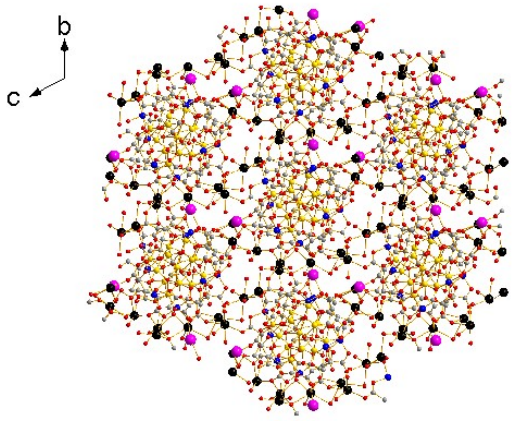

Figure S3. Ball-and-stick representation the 3D supramolecular assembly of D-**1** viewed along *a*-axis. (Cu^{II} blue, Mn^{III} yellow, Mn^{II} green, O red, C gray, Na black, K pink, hydrogen atoms omitted for clarity)

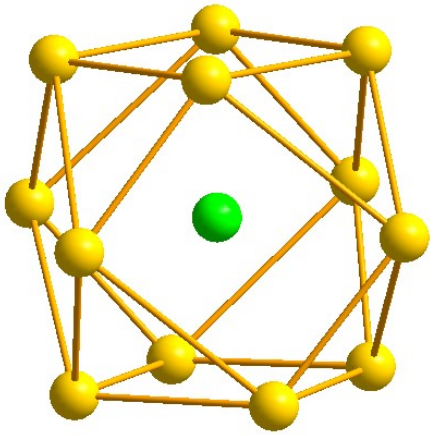

Figure S4. The $\{Mn_{12}\}$ irregular tetradecahedron with a central MnII in D-**1**. (Mn^{III} yellow, Mn^{II} green)

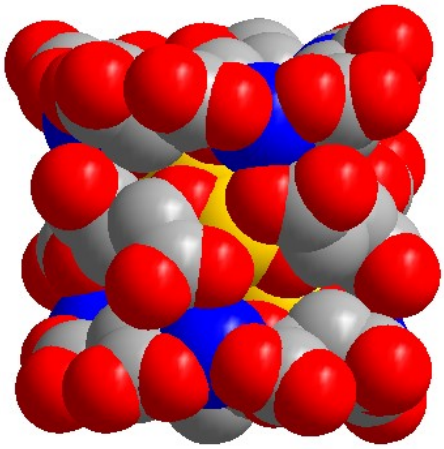

Figure S5. Space-filling representation of D-**1**. (Cu^{II} blue, Mn^{III} yellow, Mn^{II} green, O red, C gray, hydrogen atoms omitted for clarity)

Section 3: Supplementary Physical Characterization

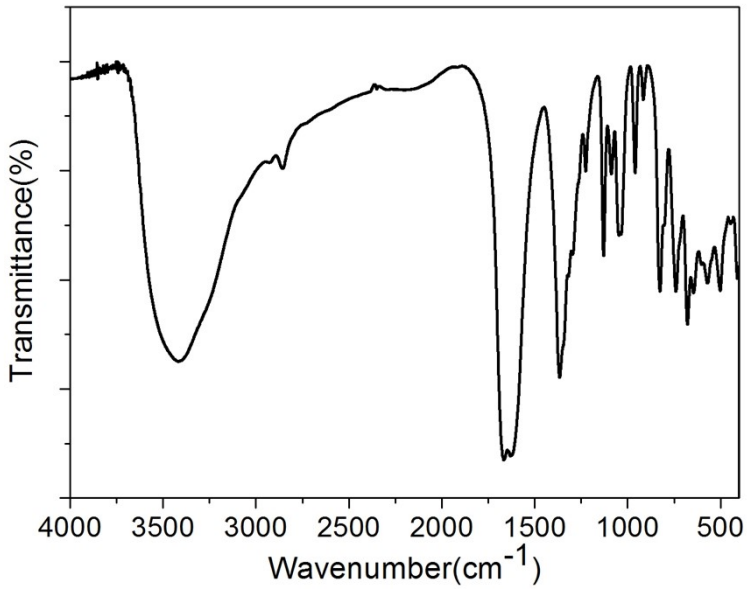

Figure S6. IR spectrum of L-**1**.

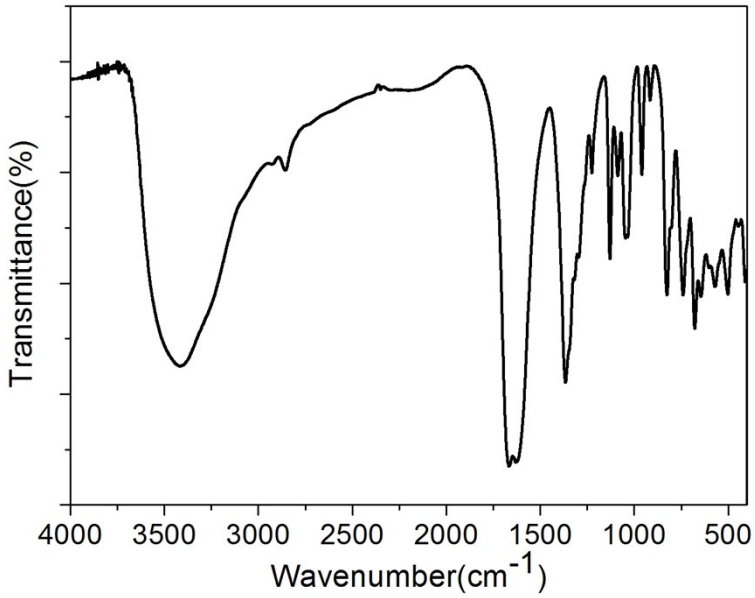

Figure S7. IR spectrum of D-**1**.

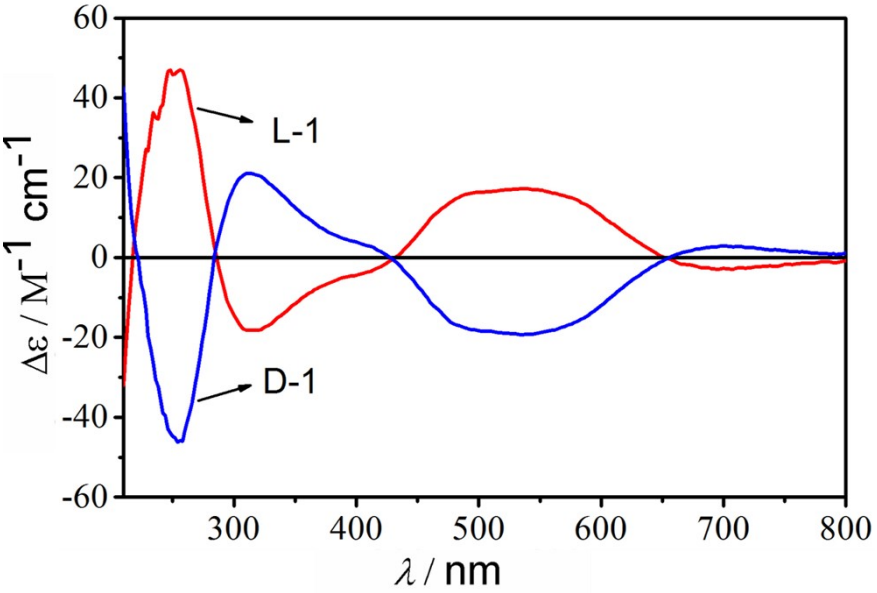

Figure S8. CD spectra of L-**1** and D-**1** in a 0.5 M NaOAc/HOAc buffer solution at pH 5.5.

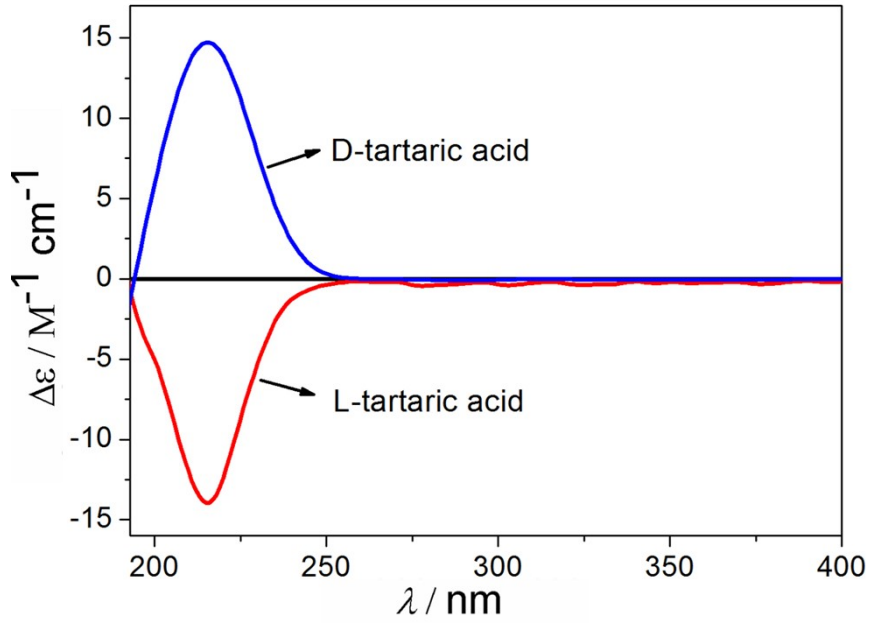

Figure S9. CD spectra of L-(+)- and of D-(-)-tartaric acid in water.

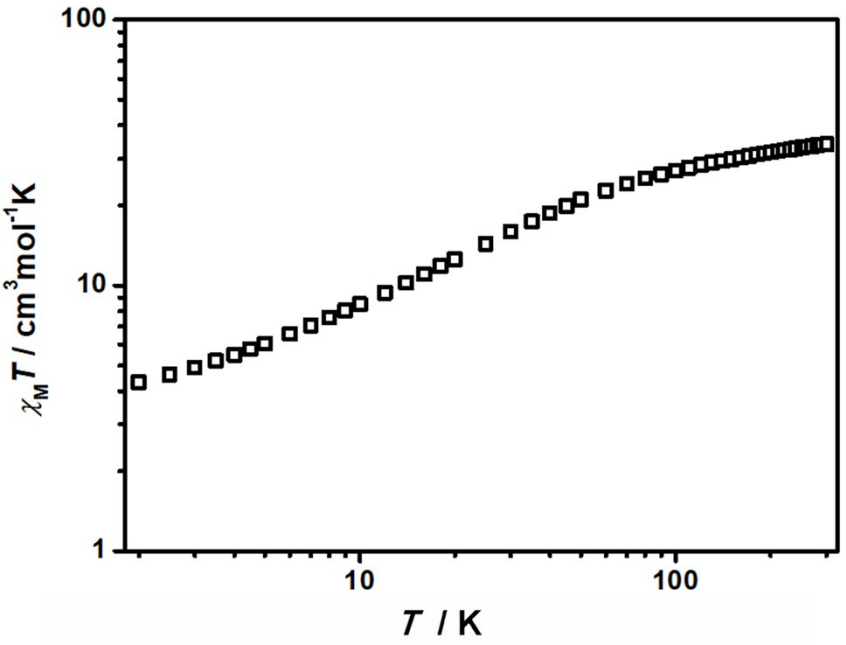

Figure S10. Variable temperature dc susceptibility data for D-**1** in a field of 2000 Oe from 2 – 300 K in log scale.

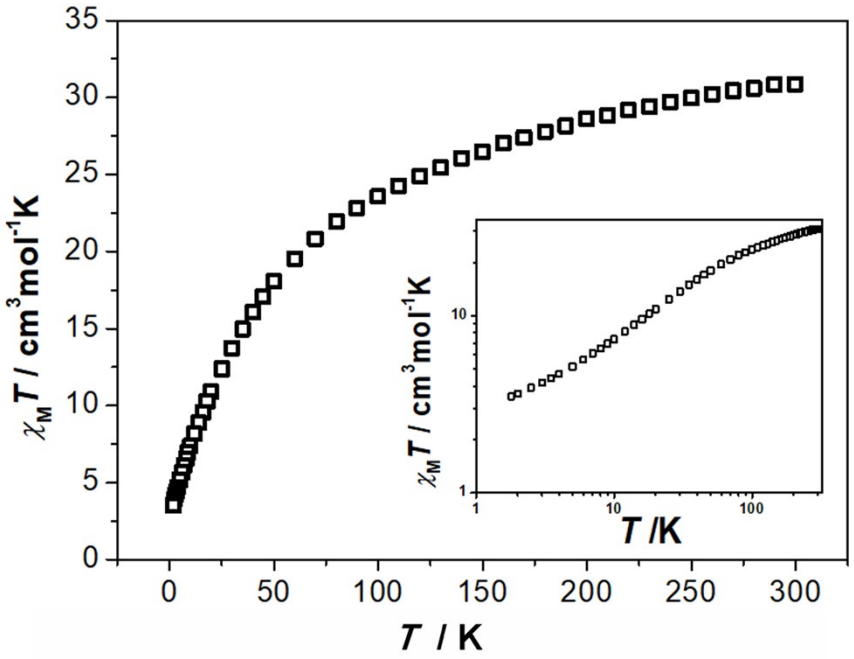

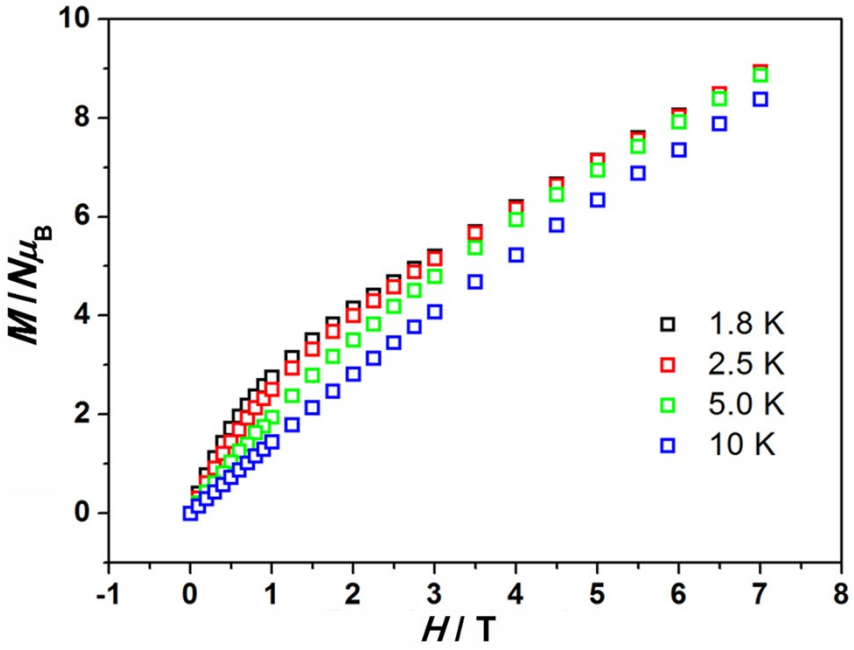

Figure S11. Variable temperature dc susceptibility data for L-**1** in a field of 2000 Oe from 2 – 300 K (top). Magnetisation versus field plots at temperatures of 1.8, 2.5, 5.0 and 10 K for L-**1** (bottom).

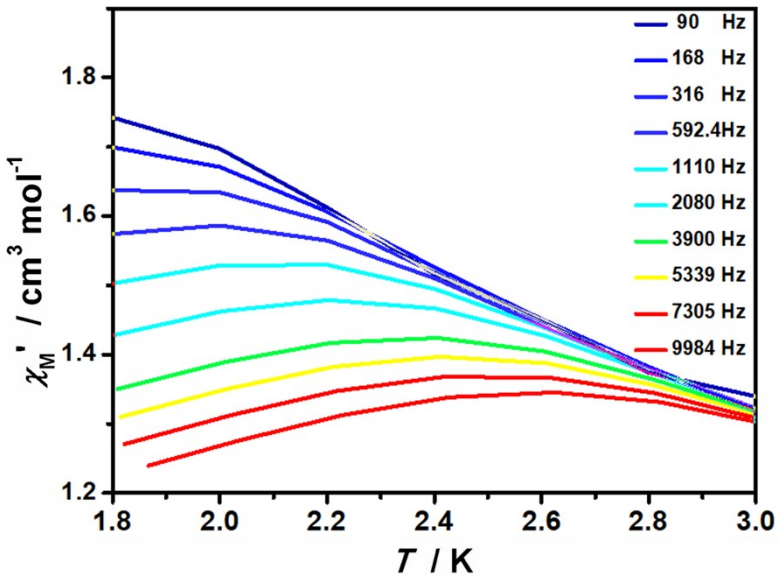

Figure S12. Temperature dependent in-phase susceptibility signals D-**1** in a 0 Oe dc applied magnetic field, in the temperature range 1.8 – 3.0 K.

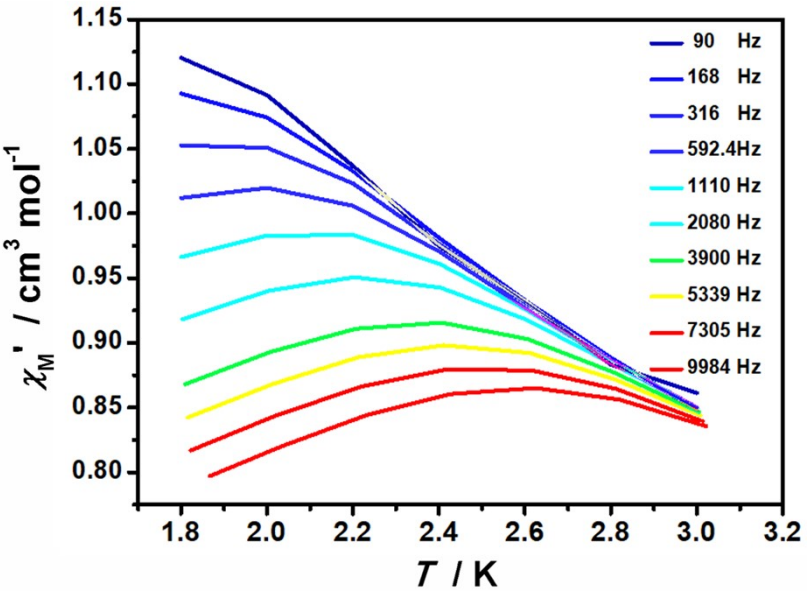
90 Hz
168 Hz
316 Hz
592.4Hz
1110 Hz
2080 Hz
3900 Hz
5339 Hz
7305 Hz
9984 Hz
χM' / cm3 mol-1
T / K

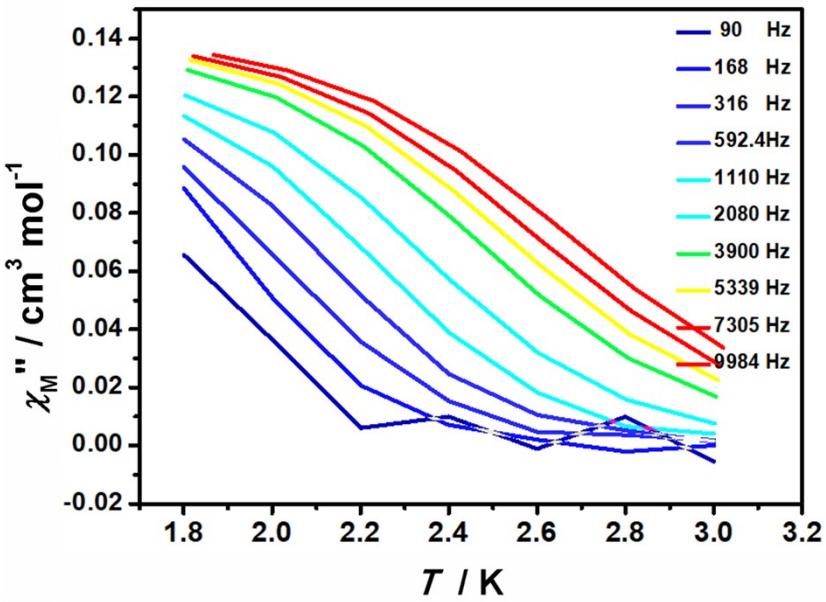
90 Hz
168 Hz
316 Hz
592.4Hz
1110 Hz
2080 Hz
3900 Hz
5339 Hz
7305 Hz
9984 Hz
χM'' / cm3 mol-1
T / K

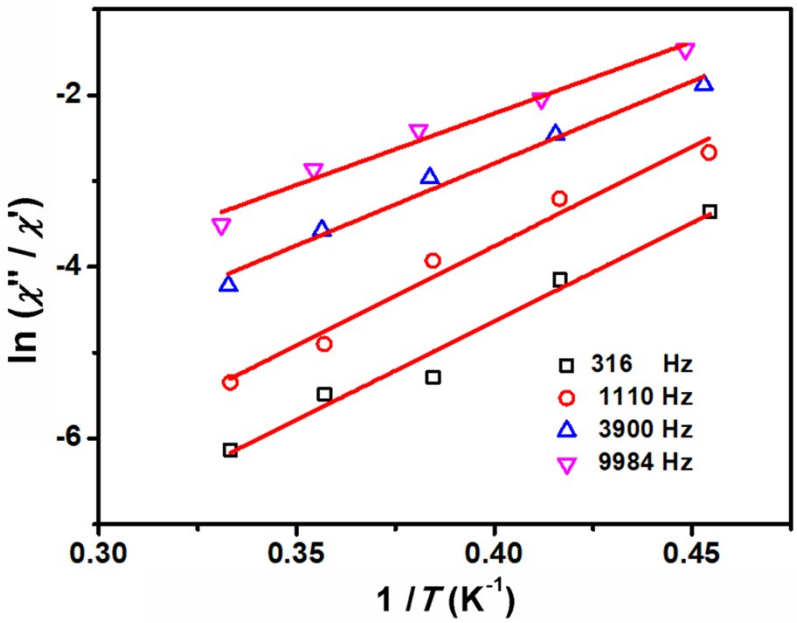

Figure S13. The temperature-dependence of in phase (top) and out-of-phase (middle) magnetization susceptibility of L-**1** at different frequencies by SQUID VSM. The reversed energy barrier fitting plot with $\ln(\chi'' / \chi') = \ln(\omega\tau_0) + U/k_BT$ (bottom). The energy barrier is ca. U =19 (±4) K and τ_0 = 2.0 (± 0.3) × 10^{-9} s.

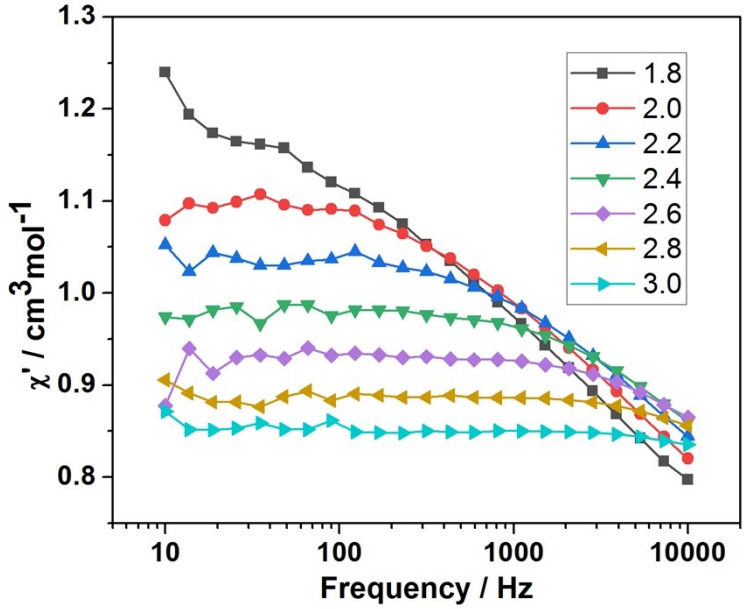

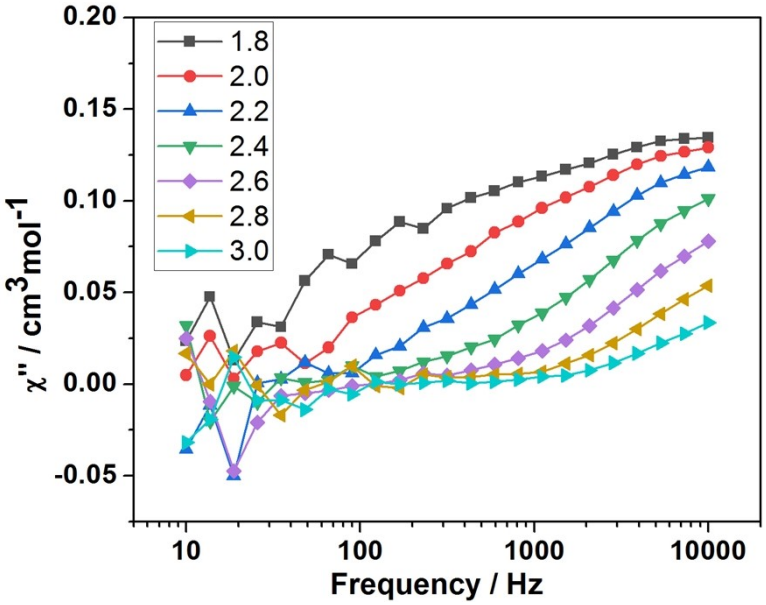

Figure S14. Frequency dependent in-phase (top) and out-of-phase (bottom) susceptibility signals for L-**1** in a 0 Oe dc applied magnetic field, in the temperature range 1.8 – 3.0 K.

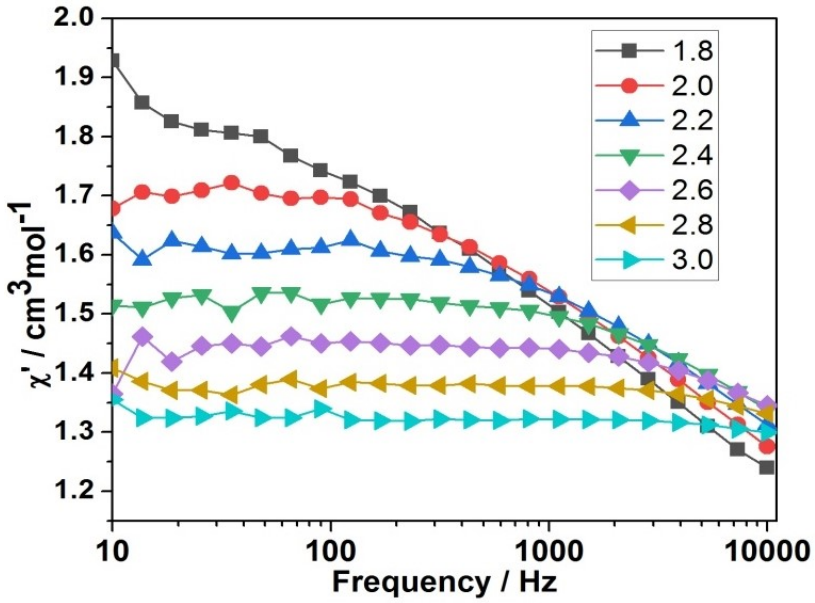

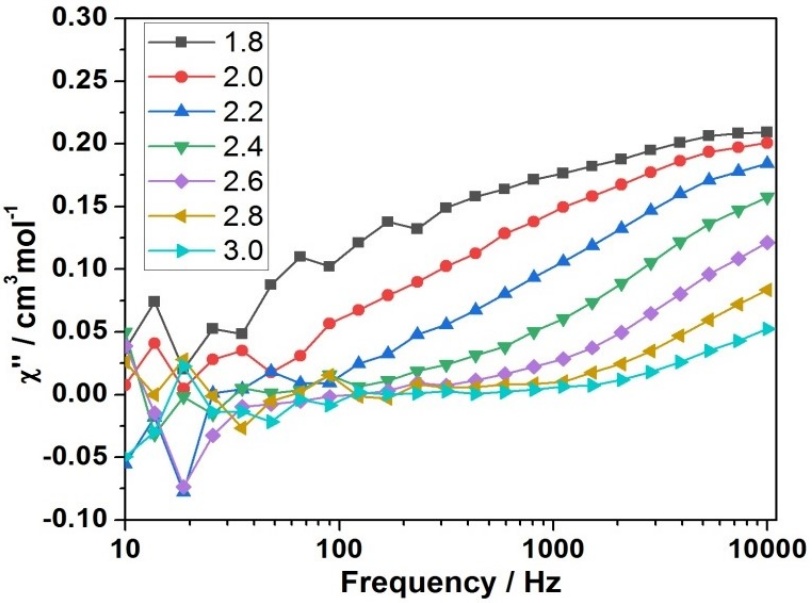

Figure S15. Frequency dependent in-phase (top) and out-of-phase (bottom) susceptibility signals for D-**1** in a 0 Oe dc applied magnetic field, in the temperature range 1.8 – 3.0 K.

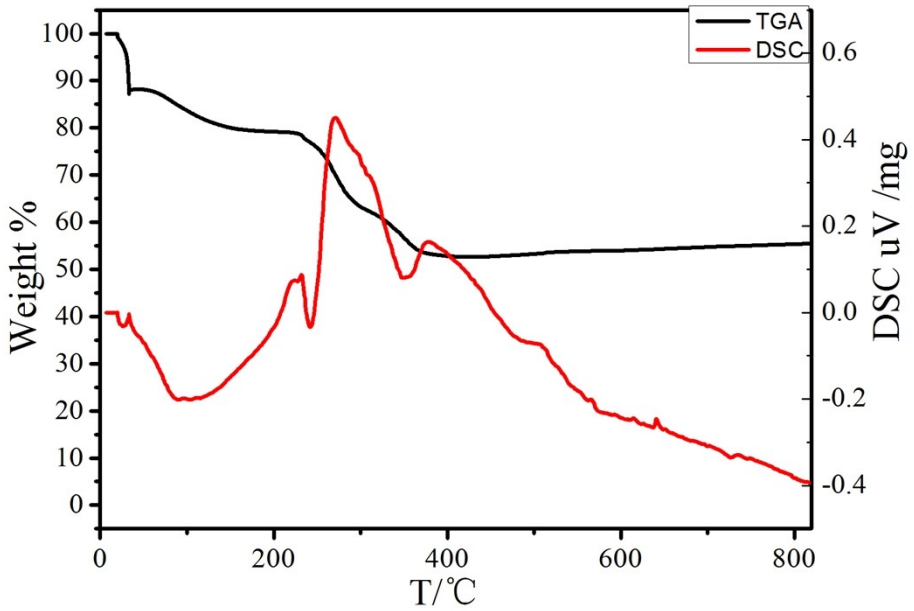

Figure S16. TGA of L-**1**.

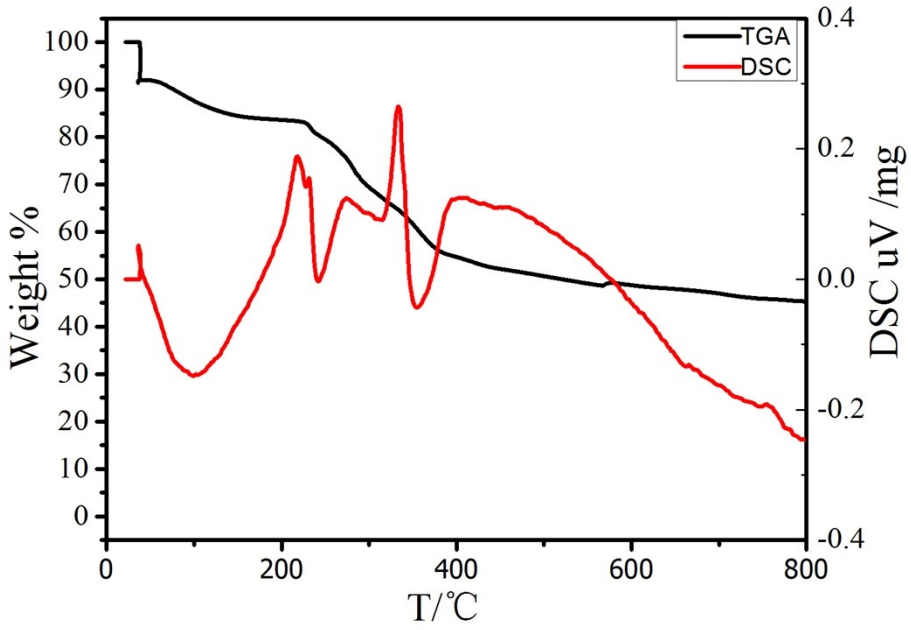

Figure S17. TGA of D-**1**.

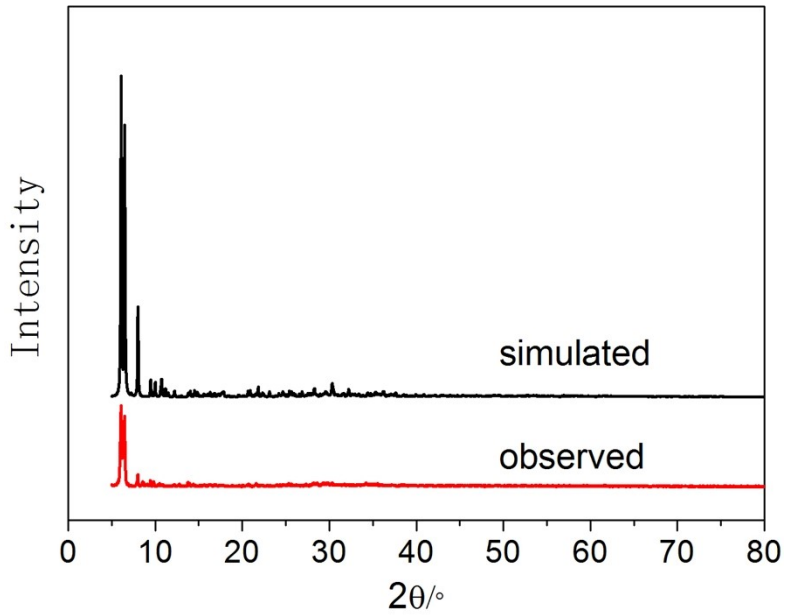

Figure S18. Simulated and observed powder X-ray diffraction (PXRD) of L-**1**.

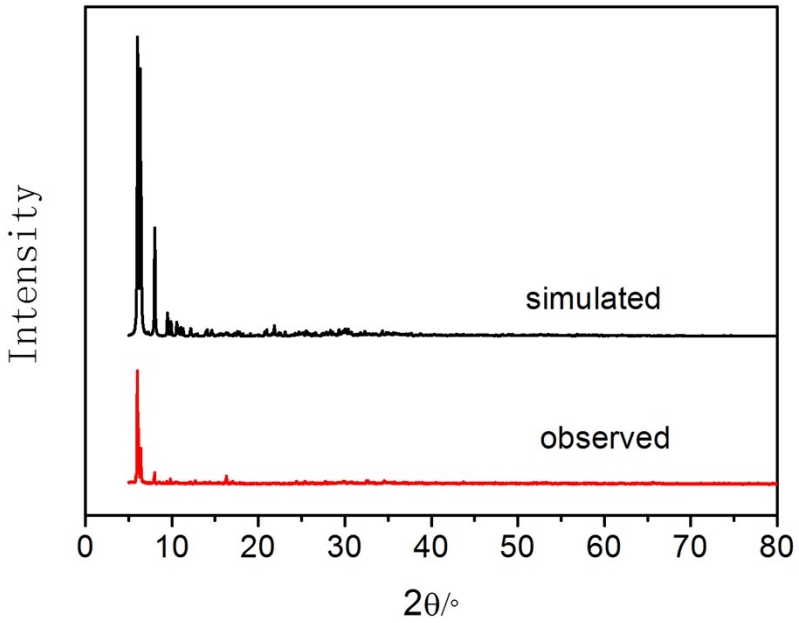

Figure S19. Simulated and observed powder X-ray diffraction (PXRD) of D-**1**.

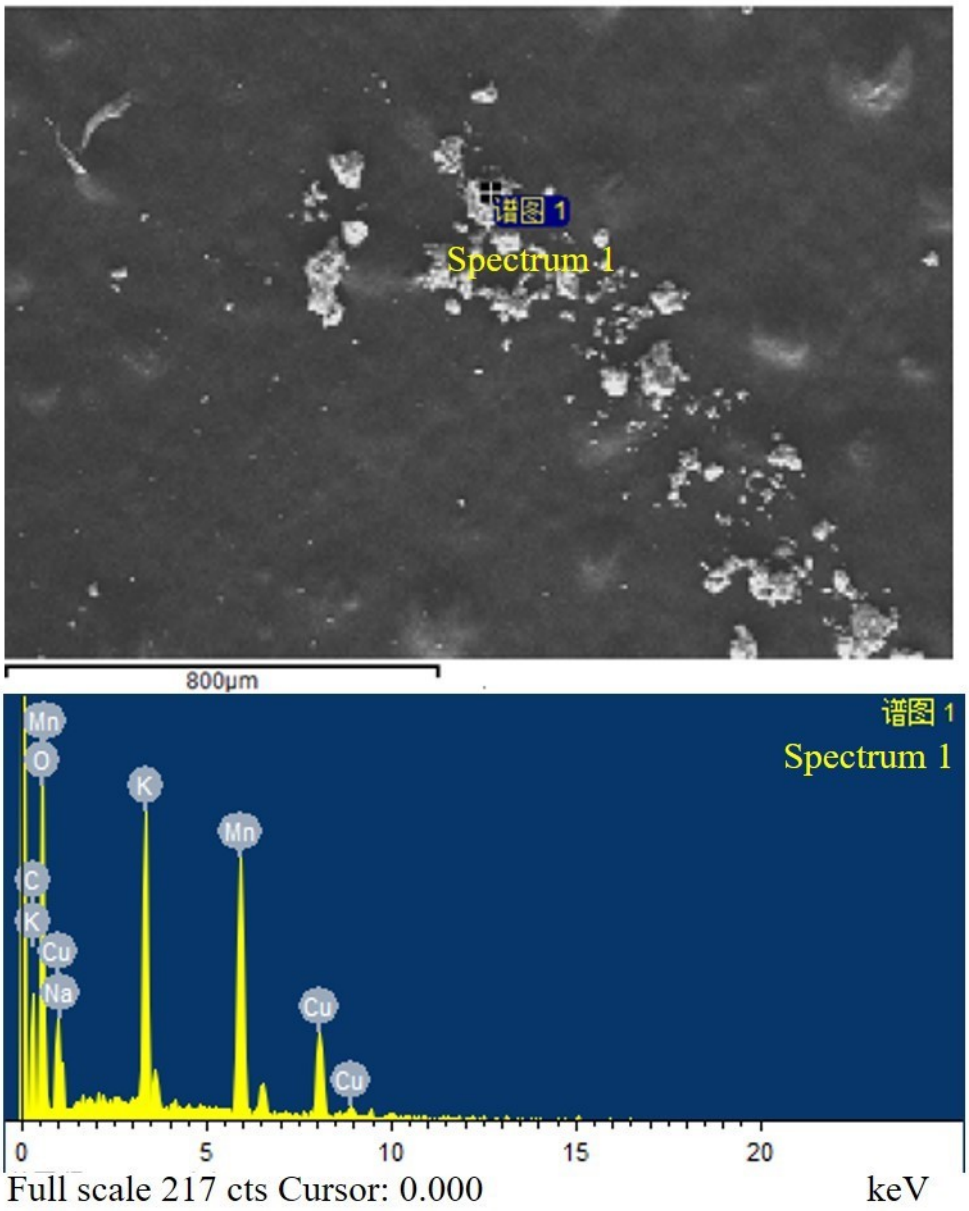

Figure S20. The EDS characterization for L-**1**.

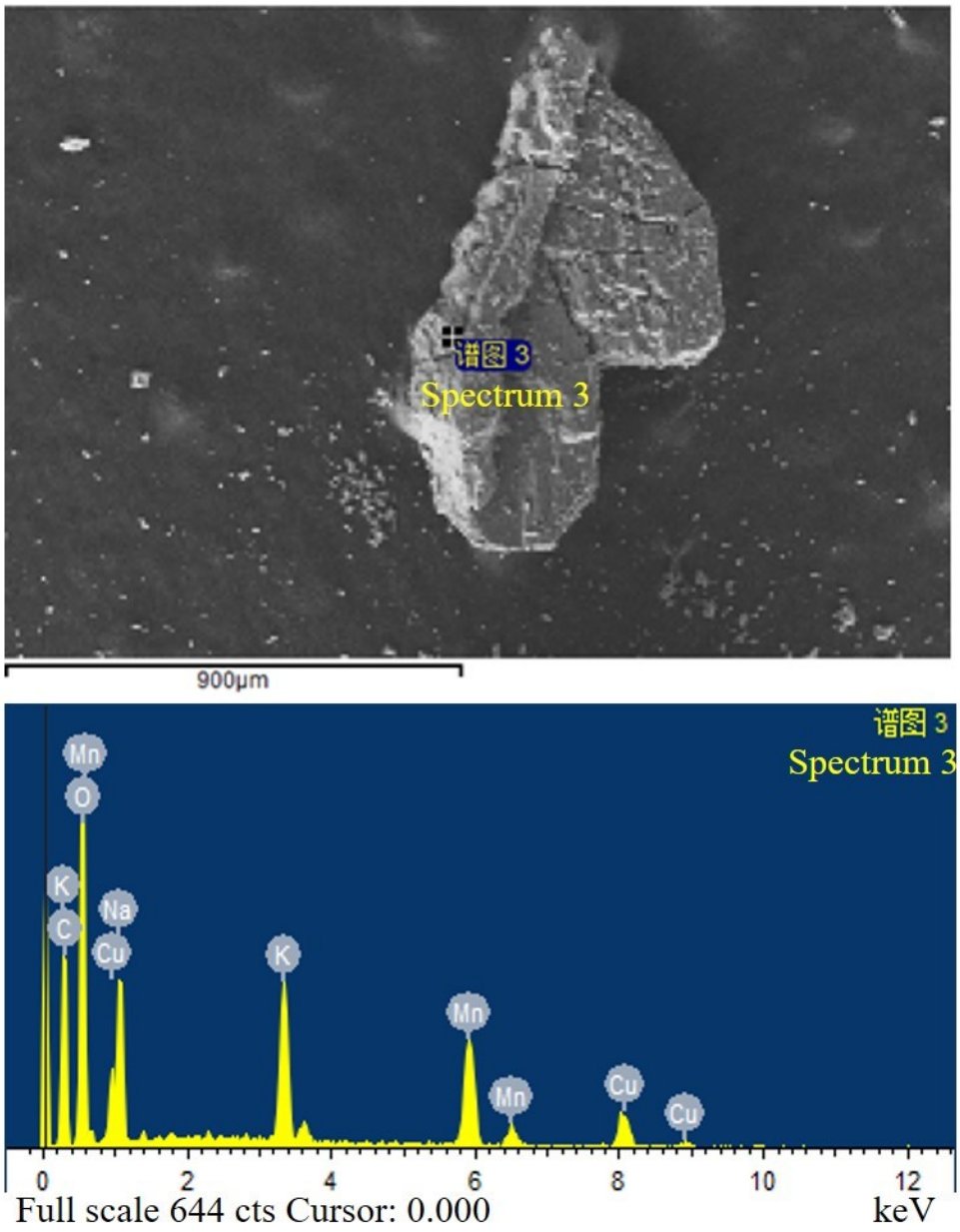

Figure S21. The EDS characterization for D-**1**.

Table S3. Selected bond distances (Å) and bond angles (°) in L-1

	Å		Å		Å		Å		°
Mn1-075	2.325	Mn4-019	1.8759	Mn7-081	1.8690	Mn10-019	1.9109	05-Mn1-039	76.222
Mn1-019	2.3708	Mn4-075	1.8851	Mn7-086	1.8862	Mn10-024	1.9510	019-Mn1-041	76.972
Mn1-077	2.345	Mn4-014	1.9120	Mn7-084	1.9422	Mn10-065	2.1305	033-Mn2-074	92.375
Mn1-041	2.3364	Mn4-012	1.9382	Mn7-0122	2.1173	Mn10-073	2.4737	072-Mn2-079	95.426
Mn1-079	2.3597	Mn4-0120	2.1621	Mn7-037	2.6506	Mn11-0122	1.8758	048-Mn6-050	81.740
Mn1-039	2.3536	Mn4-073	2.5122	Mn8-039	1.8883	Mn11-065	1.8921	073-Mn6-075	79.959
Mn1-081	2.3591	Mn5-0110	1.8786	Mn8-038	1.8883	Mn11-019	2.0383	041-Mn7-081	90.421
Mn2-041	1.8826	Mn5-0120	1.8935	Mn8-077	1.8947	Mn11-0123	2.0458	086-Mn7-0122	94.528

Mn2-074	1.8967	Mn5-075	2.0680	Mn8-036	1.9541	Mn11-0116	2.1042	038-Mn8-039	95.195
Mn2-079	1.9074	Mn5-0112	2.0714	Mn8-071	2.1294	Mn11-041	2.1247	036-Mn8-077	97.056
Mn2-072	1.9344	Mn5-104	2.0771	Mn8-073	2.5626	Mn12-079	1.8786	09-Mn9-039	97.86
Mn2-033	2.1386	Mn5-081	2.1069	Mn9-0108	1.8910	Mn12-05	1.8873	09-Mn9-0100	101.528
Mn2-037	2.5501	Mn6-039	1.8864	Mn9-09	1.8946	Mn12-062	1.9000	024-Mn10-065	98.004
Mn3-033	1.8784	Mn6-075	1.9028	Mn9-039	2.0649	Mn12-060	1.9513	073-Mn10-077	80.965
Mn3-071	1.8820	Mn6-050	1.9097	Mn9-0100	2.0838	Mn12-09	2.1416	069-Mn9-0100	96.51
Mn3-079	2.0627	Mn6-048	1.9422	Mn9-05	2.0959	Mn12-037	2.4992	0100-Mn9-0108	80.315
Mn3-063	2.0748	Mn6-0108	2.1436	Mn9-069	2.1202	Mn13-05	1.8724	05-Mn13-037	77.846
Mn3-077	2.0861	Mn6-073	2.4646	Mn10-077	1.8859	Mn13-098	1.9064	096-Mn13-098	80.898
Mn3-067	2.1264	Mn7-041	1.8616	Mn10-026	1.9075	Mn13-096	1.9304	096-Mn13-037	92.641